Hydrogen-Induced Effects in Alloys of Type $Nd_2(Fe/Co)_{14}B$ Studied by X-ray Photoelectron Spectroscopy

D. Lebiedz,[†] H. Züchner,*[,†] and O. Gutfleisch[‡]

Institut für Physikalische Chemie, Corrensstrasse 30, 48149 Münster, Germany, and Institut für Metallische Werkstoffe, IFW Dresden, Postfach 27 01 16, D-01171 Dresden, Germany

Received November 26, 2002. Revised Manuscript Received April 5, 2004

Hydrogen-induced effects in alloys of type $Nd_2(Fe_xCo_{1-x})_{14}B$ have been investigated by X-ray photoelectron spectroscopy (XPS). Conclusions are drawn regarding the different behavior during the HDDR process (*hydrogenation, disproportionation, desorption, recombination*) upon substitution of Fe by Co. This hydrogen-induced fully reversible process is applied to produce highly coercive magnet powders. The XPS data provide information on the effect of different alloy components on hydrogen adsorption at the surface and absorption into the bulk as well as hydrogen-induced disproportionation and phase transformation in the course of the HDDR process. Specific differences in surface composition and oxidation behavior for the Fe and Co system, which are influenced by the presence of hydrogen, seem to play a major role in the primary steps of hydrogenation and disproportionation. In addition, hydrogen-induced electronic effects induced by "surface hydrogenation by ion implantation" under UHV conditions, which inter alia avoids surface contamination usually accompanying hydrogenation processes in an external chamber, have been studied. The XPS data allow us to explain changes of special properties of the $Nd_2(Fe_xCo_{1-x})_{14}B$ systems, such as fundamental aspects of hydrogen adsorption on the metal surface and hydrogenation and disproportionation.

1. Introduction

Alloys of the type $Nd_2(Fe_xCo_{1-x})_{14}B$ undergo phase transformations when heat treated in hydrogen atmosphere. At ∼420 K and 1 bar hydrogen pressure, the bulk alloy decrepitates into a coarse-grained powder due to volume expansion upon hydrogen absorption on interstitial sites.[1] This hydrogen decrepitation process is widely used to ease powder production for the synthesis of rare earth−transition metal permanent magnets, in particular, high-performance Nd−Fe−B-type sintered magnets.[2] At higher temperatures, a hydrogen-induced reaction can take place: a fully reversible phase transformation leads to substantial grain refinement of the parent phase. In the case of $Nd_2Fe_{14}B$, a submicrometer grain-sized powder is the result. This highly coercive material can be used to prepare both bonded and hot pressed magnets.[3] Above 920 K, hydrogenated $Nd_2Fe_{14}B$ disproportionates into neodymium hydride, α-iron, and ferroboron.[4] By further annealing under vacuum at 1070 K, the reverse reaction takes place and the disproportionated mixture of Nd−Fe−B recombines under hydrogen desorption. The complete process is described as HDDR (*hydrogenation, disproportionation, desorption, recombination*).[5] A unique feature of the HDDR process is the possibility of producing magnetically anisotropic powder, which can be used for the preparation of highly textured magnets.[2,6] Alloy substitutions by other elements such as Co are of particular relevance for optimizing final magnet properties when at the same time the HDDR processing conditions, in particular temperature and hydrogen pressure, are adjusted accordingly.[6−8] The partial substitution of iron by cobalt stabilizes the starting alloy with respect to disproportionation; i.e., more severe conditions are required to achieve decomposition. Consequently, under standard conditions, such as atmospheric hydrogen pressure, hydrogen absorption peaks become weaker and absorption kinetics become slower as the Co contents of the alloys increase[9] (Figure 1). Thus, reactive hydrogen milling or high hydrogen pressure disproportionation is necessary to disproportionate the thermodynamically very stable $Nd_2Co_{14}B$.[10]

It was demonstrated that the decrepitation of the hydrogenated alloys can be avoided in an s(*solid*)-HDDR process by introducing hydrogen at elevated temperature instead of heating the system in hydrogen atmo-

* To whom correspondence should be addressed. E-mail:zuchner@uni-nuenster.de.
[†] Institut für Physikalische Chemie.
[‡] IFW Dresden.

(1) McGuiness, P. J.; Devlin, E. J.; Harris, I. R.; Rozendaal, E.; Ormerod, J. *J. Mater. Sci.* **1987**, *24*, 2541.
(2) Gutfleisch, O.; Harris, I. R. *J. Phys. D: Appl. Phys.* **1996**, *29*, 2255−2265.
(3) Takeshita, T.; Nakayama, R. In *Proc. 10th Int. Workshop on Rare-Earth Magnets and their Applications*, Kyoto, Japan. 1989; p 551.
(4) Codogan, J. M.; Coey, J. M. D. *Appl. Phys. Lett.* **1986**, *148*, 442.
(5) McGuiness, P. J.; Zhang, X. J.; Yin, X. J.; Harris, I. R. *J. Less-Common Met.* **1990**, *158*, 359.
(6) Takeshita, T.; Nakayama, R. In *Proc. 11th Int. Workshop on Rare-Earth Magnets and their Applications*, Kyoto, Japan, 1990; p 49.
(7) Nakurama, H.; Suefuji, R.; Sugimoto, S.; Okada, M.; Homma, M. *J. Appl. Phys.* **1994**, *76*, 6828.
(8) Sugimoto, S.; Gutfleisch, O.; Harris, I. R. *J. Alloys Compd.* **1997**, *260*, 284.
(9) Fujita, A.; Harris, I. R. *IEEE Trans Magn.* **1994**, *30*, 860.
(10) Bollero, A.; Gutfleisch, O.; Kubis, M.; Müller, K.-H.; Schultz, L. *Acta Mater.* **2000**, *48*, 4929.

10.1021/cm021369l CCC: $27.50
Published on Web 07/14/2004

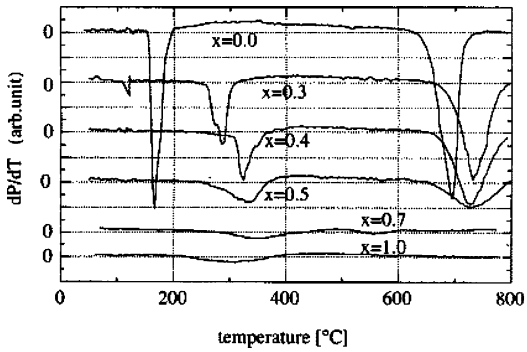

Figure 1. Hydrogen pressure change in the chamber of a TPA system as a function of temperature (heating rate, 5 K/min) during HDDR processing of alloys of type $Nd_2(Fe_{1-x}Co_x)_{14}B$ (adapted from ref 9).

sphere.[11] Based on this s-HDDR process, the application of surface analysis for reactivity studies of these materials with hydrogen forms a fundamentally new approach.

Several studies have been performed to identify microstructural changes during the HDDR treatment resulting in phase transformations and highly coercive materials. It has been shown by TEM that the disproportionation process results in $NdH_{2\pm x}$ rods embedded in an α-Fe matrix,[12] both of which have the same zone axis and crystal plane. At the initial stage, the reaction starts at a Nd-rich grain boundary phase, which activates hydrogen absorption[13−16] and acts as a fast diffusion path for hydrogen. The reaction then proceeds to the center of the matrix grains involving complex diffusion mechanisms, where Fe diffusion is presumed to be the rate-controlling factor.

In the present work, we apply X-ray photoelectron spectroscopy (XPS) to study the effect of the different alloy components on hydrogen uptake and the early stages of disproportionation in alloys of type $Nd_2(Fe_xCo_{1-x})_{14}B$, $x = 1$, 0.75, 0.5, 0. In particular, due to the high surface sensitivity of this technique, surface-related effects are especially highlighted. We analyze alloys that were processed under hydrogen atmosphere at temperatures of primary hydrogen absorption (see Figure 1) and at temperatures of disproportionation quenched after short times. Furthermore, we apply a special deuterium ion implantation technique to hydrogenate the alloys in situ under UHV conditions directly in the analysis chamber. By applying this technique, one and the same sample is investigated before hydrogenation (hydrogen-free sample) and immediately after hydrogenation under exactly identical conditions of temperature, sample probing position, gas composition, etc. The photoelectron spectra yield information on the energy and density of electronic states and the relative distribution of the alloy components, which allow a better insight into the microscopic steps of the HDDR process. The results will be augmented by a detailed analysis of depth profiles obtained via Ar ion sputtering.

2. Experimental Section

2.1. Preparation of Nd−Fe/Co−B Alloys. The $Nd_2(Fe_xCo_{1-x})_{14}B$ ($x = 1$, 0.75, 0.5, 0) samples have been prepared by inductively coupled melting of elemental Nd, Fe, Co, FeB, and CoB (purities 99.9%) with subsequent homogenization at 1323 K for 96 h. Further details were reported previously.[10] Using this starting material, we cut cubes of 0.2 cm^3 using an Isomet 4000 machine (Wirtz-Bühler) with a diamond-coated cutting wheel (4000 rpm). The slices were polished using diamond paste and afterward degreased carefully in acetone and methanol using ultrasonic cleaning. All samples analyzed in this work, including the reference samples for XPS measurements, were prepared and treated like this.

2.2. External Hydrogenation Treatment. The slices were treated in a hydrogenation chamber consisting of a quartz glass tube, an electric heater, and a UHV pumping device equipped with a hydrogen gas inlet valve. Before starting the hydrogenation, the glass tube containing the alloys was evacuated for ∼12 h to a basis pressure of $<5 \times 10^{-5}$ mbar. In analogy to the s-HDDR process, the system was heated under vacuum at 423 ($Nd_2Fe_{14}B$) or 573 K ($Nd_2Co_{14}B$) for 1.5 h and then the chamber was hydrogen filled to a pressure of 800 mbar. Fifteen minutes after hydrogen filling, the system was quickly cooled to room temperature under hydrogen atmosphere, and the samples were transferred directly into the UHV system of the XP spectrometer and analyzed immediately. As in the s-HDDR process, this special heat treatment avoids a decrepitation of the material, which would impose some difficulties on the application of surface spectroscopic methods. Here, no decrepitation is observed if cooling to room temperature is quick enough in the presence of H_2.

2.3. Partial Disproportionation. The metal slices were treated in the hydrogenation chamber at 800 mbar hydrogen pressure and 1073 K. Under these conditions, the disproportionation reaction begins for Fe-rich alloys. After 10 min, the reaction was stopped by quickly cooling the system to room temperature.

2.4. XPS Measurements. XP spectra were acquired using a Kratos Axis Ultra combined Auger/photoelectron spectrometer equipped with a monochromized Al Kα X-ray source, a hemispherical analyzer with energy resolution of 0.55 eV at pass energy of 40 eV, and an eight channeltron photomultiplier. The XPS data were evaluated and modified for presentation using the Kratos Vision 2 processing software. In all cases, the raw spectra were used without smoothing. Peak integration was performed in all cases after subtracting Shirley background,[17] and all component fittings are based on Gaussian functions as representatives for single components and the application of simplex algorithm for optimal fitting. For depth profiles Ar^+ ion sputtering (Minibeam I ion gun, $j = 1.5 \times 10^{-6}$ A cm^{-2}) was applied. XPS measurements were carried out at room temperature.

(11) Gutfleisch, O.; Martinez, N.; Verdier, M.; Harris, I. R. *J. Alloys Compd.* **1994**, *215*, 227.
(12) Gutfleisch, O.; Matzinger, M.; Fidler, J.; Harris, I. R. *J. Magn. Magn. Mater.* **1995**, *147*, 320.
(13) Harris, I. R.; McGuiness, P. J.; Jones, D. G. R.; Abell, J. S. *Phys. Scr.* **1989**, *T19*, 435.
(14) McGuiness, P. J.; Harris, I. R.; Scholtz, U. D.; Nagel, H. *Z. Phys. Chem. N. F.* **1989**, *163*, 687.
(15) Williams, A. J.; McGuiness, P. J.; Harris, I. R. J. *Less-Common Met.* **1991**, *171*, 149.
(16) Book, D.; Harris, I. R. *J. Alloys Compd.* **1995**, *221*, 187.
(17) Shirley, D. A. *Phys. Rev. B* **1972**, *5*, 4709.

Table 1. Component Quantification (%) for Nd and Fe Spectra in Figure 4

	Nd $3d_{5/2}$	Nd $3d_{5/2}$ ox	Nd $3d_{5/2}$ sat	O KLL	Fe $2p_{5/2}$	Fe $2p_{5/2}$ ox
hydrogen free	18.71	42.95	16.95	21.39	26.14	73.86
hydrogenated	19.75	30.05	18.86	31.33	2.15	97.85

Table 2. Energy Differences (Distance between Peak Maximums Nd 3d, Fe 2p and Co 2p: Δ Nd 3d − Fe 2p/Co 2p) Depending on Alloy Composition

	pure components (distinct XPS spectra of pure Nd, Fe, and Co)	$Nd_2Co_{14}B$	$Nd_2Fe_{14}B$	$Nd_2Co_{14}B$ (after D_2^+ ion implantation)	$Nd_2Fe_{14}B$ (after D_2^+ ion implantation)
Δ Nd 3d − Fe 2p (eV)	273.98		274.23		274.05
Δ Nd 3d − Co 2p (eV)	202.59	202.97		202.79	

2.5. In Situ Hydrogen (Deuterium) Ion Implantation. Hydrogenation and surface cleaning were performed simultaneously directly in the XPS analysis chamber by ion bombardment (∼15 min) using an Ar/D_2 gas mixture (volume 1:1). (Sputtering with pure D_2 is much less effective to remove surface contaminations substantially and therefore inappropriate for analyzing hydrogen-induced electronic effects. We normally use D_2 instead of H_2 for "hydrogen" implantation, especially in SIMS experiments.[24] The kind of the hydrogen isotope has no influence on the effects to be studied in this paper; i.e., isotope effects are negligible. The application of the in situ hydrogenation technique enables the observation of changes in the XP spectra including chemical shifts of peaks, which are caused only by deuterium but nearly unaffected by other components such as oxygen. XP spectra of the deuterium-loaded sample were acquired immediately after sputtering in order to avoid excessive hydrogen loss. An only rough estimation based on the implantation parameters yields deuterium concentrations in the probing depth of the sample of ∼30 atom %. Comparable concentrations should be obtained also by the external hydrogen loading procedure.

3. Results and Discussion

The XPS investigations were performed to obtain information about the effect of the different alloy components and the thermodynamic stability of the alloys toward the hydrogenation reaction. For this purpose, chemical shifts of energy levels due to electronic effects as well as surface compositions and depth profiles have been analyzed. Since the effects caused by hydrogen/deuterium uptake on the XP spectra are small, we mainly discuss energy differences in the spectra and compare results from samples that have been treated and investigated under almost identical and comparable conditions, as far as it is possible. Data and trends reported here have also been proved regarding the reproducibility successfully.

3.1. Nonhydrogenated Compounds. First, the relative peak positions and energy differences of Nd 3d and Fe 2p/Co 2p in XP spectra of nonhydrogenated (and hydrogenated) samples of $Nd_2Fe_{14}B$, $Nd_2(Fe_{0,5}Co_{0,5})_{14}B$, $Nd_2Co_{14}B$, and pure Nd, Fe, and Co as references have been determined in order to quantify electronic effects that affect the thermodynamic stability of the alloys $Nd_2(Fe_xCo_{1-x})_{14}B$. Prior to analysis, all samples were cleaned by Ar sputtering. The peak maximums were carefully determined from the zero-crossing of the first derivative spectra. In this way, even small electronic effects could be determined. Table 2 shows the results and gives an idea of how thermodynamic stability might be related to electric charge distribution in the alloys.

As expected from an initial-state picture based on charge transfer from the electropositive (Nd) to the more electronegative component (Fe or Co), the energy differences Δ Nd 3d − Fe 2p/Co 2p increase in all of the alloys in relation to the pure components. This effect can be explained by the formation of a polar chemical bond $Nd^{\delta+}Me^{\delta-}$ (Me = Fe, Co), which is stronger for those alloys with Me = Co and therefore leads to a more positive chemical shift for the Nd−Co−B alloy. In $Nd_2Co_{14}B$, the energy difference Δ Nd 3d − Co 2p differs by 0.38 eV from that in the spectra of pure Nd and Co, whereas in $Nd_2Fe_{14}B$, Δ Nd 3d − Fe 2p differs only by 0.25 eV from the values of pure Nd and Fe. The corresponding relations in $Nd_2(Fe_{0,5}Co_{0,5})_{14}B$ (not shown) confirm the observation that the Nd−Co bond seems to be more polar than the Nd−Fe one by a factor of 1.5. Additionally, in alloys containing both Fe and Co, the overall polarity of the Nd−Me bonds is obviously equalized. This may be due to an Fe−Co interaction of nonnegligible strength. The direction of the observed shift is opposite to what would be expected when considering final-state effects for lanthanides alloyed with transition metals as proposed by Mårtensson and Nilsson[18] and Nilsson et al.[19] This means that for the system Nd−Fe/Co−B initial-state effects seem to dominate final-state effects in the photoelectron emission process.

3.2. D_2^+ Ion Implanted Compounds. It is not possible to compare the results discussed in section 3.1 directly with those for alloys hydrogenated by the HDDR process which, unfortunately, involves partial oxygen contamination due to residual oxygen in the gas atmosphere. The chemical shifts of the corresponding peaks caused by partial oxidation mask the small hydrogen effects. Nonetheless, in D_2^+ ion implantation experiments performed under UHV conditions, it could be shown that the energy differences of Nd 3d and Fe 2p/Co 2p are reduced considerably under hydrogen influence in both $Nd_2Co_{14}B$ and $Nd_2Fe_{14}B$ by ∼0.18 eV to Δ Nd 3d − Co 2p = 202.79 eV and Δ Nd 3d − Fe 2p = 274.05 eV, the latter almost approaching the value for the pure components Nd and Fe. (Since the spectra of nonhydrogenated and hydrogenated samples were obtained under exactly the same conditions (one and the same sample is studied just prior and after in situ hydrogenation by direct ion implantation), small effects

(18) Mårtensson, N.; Nilsson, A. *J. Electron. Spectrosc. Relat. Phenom.* **1995**, *75*, 209.
(19) Nilsson, A.; Eriksson, B.; Mårtensson, N.; Andersen, J. N.; Onsgaard, J. *Phys. Rev. B* **1988**, *38*, 10357.

are observable, so that the results are absolutely reproducible and reliable.) This hydrogen-induced destabilization might give rise to the disproportionation of $Nd_2Fe_{14}B$ during HDDR treatment.

Hydrogen-induced electronic effects are supposed to occur particularly in the region just below the Fermi level E_F in the XP spectra. Electronic band structure calculations predict hydrogen-induced electronic bands due to hybridization of H 1s states with valence states of the alloy components.[20,21] We analyzed XP valence band spectra of in situ D_2^+ implanted alloys $Nd_2Fe_{14}B$ and $Nd_2Co_{14}B$. Figure 2 shows the spectra of the hydrogenated compounds together with those of the nonhydrogenated systems. The most remarkable result is a hydrogen-induced shift of the Fermi level (0.3 eV) toward higher binding energy in hydrogenated $Nd_2Fe_{14}B$ and the weak appearance of a hydrogen-induced electron band that appears as a shoulder at 6−8 eV. This hydrogen-induced band is not observable in hydrogenated $Nd_2Co_{14}B$. Additionally, the Fermi level shift is reduced to 0.2 eV in this system. It can be concluded that the D_2^+ ion implantation obviously reflects the hydrogen-binding behavior of the systems during the HDDR process (see Figure 1). The hydrogen presence causes considerable changes in the electronic structure only in $Nd_2Fe_{14}B$, whereas $Nd_2Co_{14}B$ remains rather unaffected by surface hydrogen ion implantation. Additionally, in $Nd_2Fe_{14}B$, the magnitude of the electronic effect suggests that the amount of hydrogen binding to the metal surface exceeds that in $Nd_2Co_{14}B$, thereby providing a rationale for the increased hydrogen absorption temperature and the weaker absorption peaks during the HDDR process in the Co alloy as well as the suppression of hydrogen-induced disproportionation in $Nd_2Co_{14}B$.

Further hydrogen effects become visible after subtracting the spectra of hydrogen-free and hydrogenated samples from each other (Figure 2). Whereas in the case of $Nd_2Co_{14}B$ no special features occur, in $Nd_2Fe_{14}B$, a hydrogen-induced band and a clear increase of the Nd 4f/5p and especially Fe 3d peaks can be observed. This can be due either to a hydrogen-induced change of the density of states (DOS), which may be caused by hybridization of H 1s with metal valence states, or to a change of the elemental surface composition. The latter aspect will be discussed in the context of discussion of depth profiles (section 3.5). An increase of Fe 3d peak intensity in externally hydrogenated $Nd_{20}Fe_{80}$ was already found by Narita et al.[22] It was interpreted in terms of an increase of Fe−Fe correlation; however, oxygen influence could not be excluded in those studies. A strengthened Fe−Fe bond and a reduction of the energy difference Δ Nd 3d − Fe 2p (Table 2), which almost approaches the value in the pure components Nd and Fe, may be first indications for a hydrogen-induced instability and the increased disproportionation tendency of $Nd_2Fe_{14}B$ as observed at high temperatures in the HDDR process. Sellmyer et al.[23] found from self-consistent theoretical calculations of the electronic

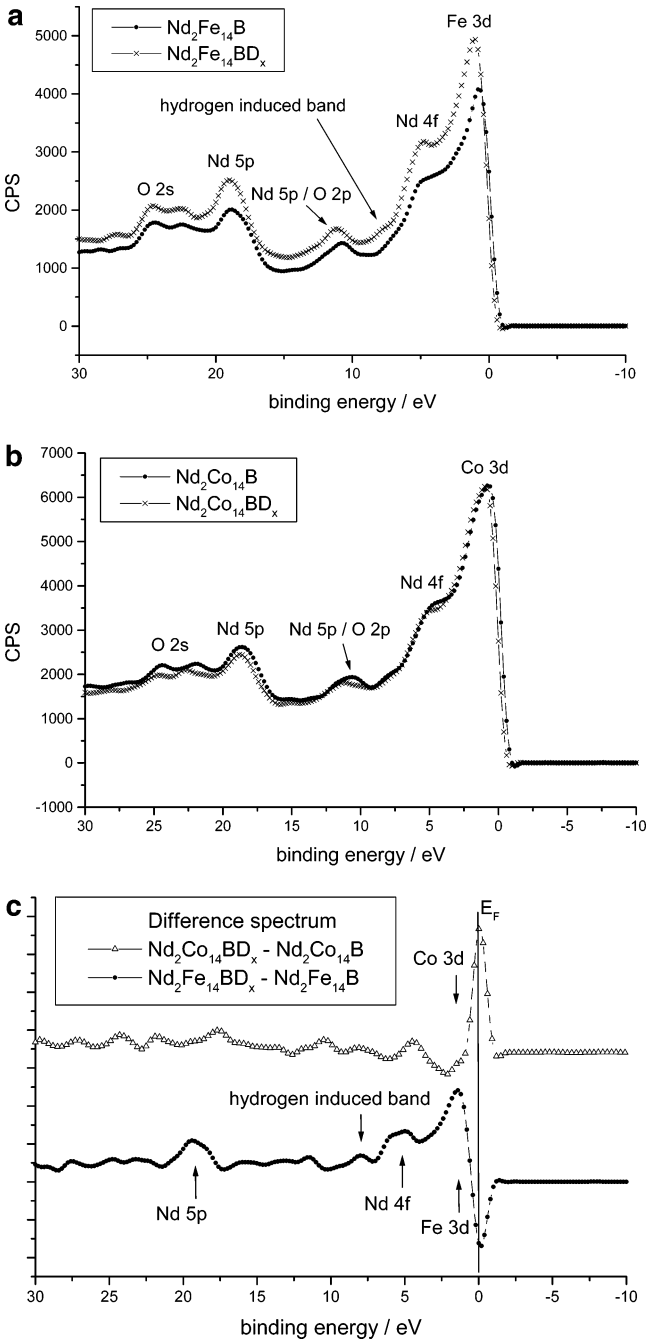

Figure 2. Hydrogen-induced electronic effects in the valence band of $Nd_2(Fe/Co)_{14}B$ after D_2^+ ion implantation: (a) $Nd_2Fe_{14}B$; (b) $Nd_2Co_{14}B$; (c) difference spectra from hydrogenated compounds in (a) and (b).

structure of $Nd_2Fe_{14}B$ that Nd 4f are quasilocalized molecular orbitals of atomlike nature. Thus, a change in the binding energy or the DOS of these states can be largely attributed to the Nd atoms themselves instead of the alloy as a whole, and the increase of Nd 4f intensity in hydrogenated $Nd_2Fe_{14}B$ may be caused by a hybridization of H 1s with Nd 4f states. This fact implies that Nd plays an important role in hydrogen surface binding in the alloy, which is confirmed by the observation of high secondary ion emission intensity of NdD_2 clusters in a secondary ion mass spectrometry analysis of the NdFe/CoB system.[24]

(20) Switendick, A. C. In *Hydrogen in Metals I*; Alefeld, G., Völkl, J., Eds.; Topics in Applied Physics 28; Springer: Berlin, 1978.
(21) Yukawa, H.; Takahashi, Y.; Morinaga, M.*Intermetallics* **1996**, *4*, S215.
(22) Narita, Y.; Yamada, M.; Tanaka, K. *Mater. Trans. JIM* **1995**, *36*, 1193.
(23) Sellmyer, D. J.; Engelhardt, M. A.; Jaswal, S. S. *Phys. Rev. Lett.* **1988**, *60*, 2077.

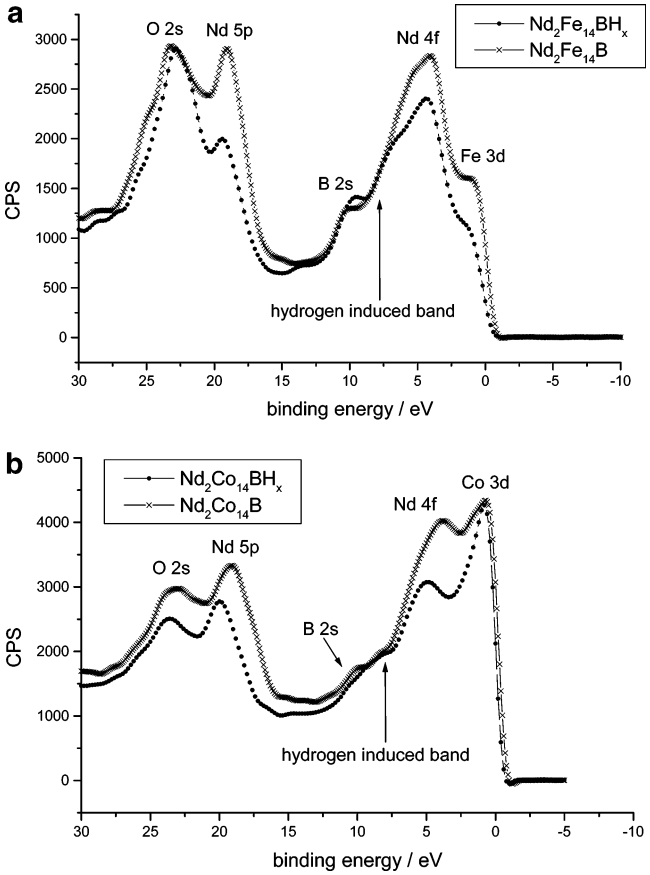

Figure 3. Hydrogen-induced changes in the valance band of $Nd_2(Fe/Co)_{14}B$, hydrogenated in 800 mbar hydrogen at 423/573 K: (a) $Nd_2Fe_{14}B$; (b) $Nd_2Co_{14}B$.

3.3. Hydrogenated Compounds (Hydrogenation Chamber, 423/573 K). In comparison with the results obtained from D_2^+ ion implanted alloys, the valence band spectra of $Nd_2Fe_{14}B$ and $Nd_2Co_{14}B$ treated in an external hydrogenation chamber (see section 2.2) have been obtained as well. No phase transformations occur at these temperatures.

XP spectra were taken from different depths for hydrogenated and hydrogen-free systems with the intention to compare only spectra from atomic layers with nearly identical (proved and controlled by O 1s and O 2s peak areas) oxygen content. Otherwise, hydrogen effects could be masked by oxygen effects. Due to small amounts of oxygen residual gas in the hydrogen atmosphere during high-temperature treatment, the hydrogenated systems contain slightly more surface oxygen than the nonhydrogenated reference alloys, which were treated in the same way as the hydrogenated ones; however, the hydrogen atmosphere was exchanged for UHV. Possibly the increased amount of surface oxygen is due to a higher reactivity of the surface hydride to oxygen.

The spectra in Figure 3 confirm the occurrence of a hydrogen-induced band at 6−8 eV as well as a small shift of the Fermi level toward higher binding energies. Both effects have already been observed in the spectra of D_2^+ ion implanted alloys (section 3.2). In Figure 3, an additional hydrogen-induced effect becomes visible. In $Nd_2Co_{14}B$, the Nd 4f and 5p peaks experience a stronger shift toward higher binding energy than expected as a result of Fermi level shift whereas the corresponding peaks in $Nd_2Fe_{14}B$ do not shift. This implies that Nd atoms are transferred to a formally higher oxidation state in hydrogenated $Nd_2Co_{14}B$, which means they are losing some electron density. This is not observed in $Nd_2Fe_{14}B$, where Nd seems to be less positively polarized as already discussed in secion 3.1 for the nonhydrogenated alloys, and although the Fe alloy is much more sensitive to oxygenation and contains a larger relative amount of surface oxygen after external hydrogenation (see O 2p peak in Figure 3a). As a conlusion, the observed shift in Nd peaks for the Co alloy is obviously not caused by oxygen.

To study the differences in surface oxidation behavior under HDDR conditions, we analyzed surface XP spectra of the alloys after hydrogenation. These spectra were acquired after only 60 s of Ar sputtering to remove only a thin contamination layer from the surface. They are compared with spectra of nonhydrogenated alloys containing nearly the same amounts of oxygen as proved by O 1s peak area comparison.

Figure 4 shows Nd 3d and Fe 2p peaks of hydrogenated and hydrogen-free $Nd_2Fe_{14}B$. Hydrogenation in the presence of small amounts of oxygen causes an unexpected oxidation behavior of the surface components in the alloy. This oxidation is due to (unavoidable) residual oxygen gas during hydrogenation, as mentioned before. The oxidation degree after hydrogenation is lower for Nd and higher for Fe than in the nonhydrogenated reference samples. The opposite behavior would be expected from reduction potentials (Nd, −2.43 V; Fe, −0.44 V). The high relative intensity of the O KLL peak in the Nd 3d spectrum of hydrogenated $Nd_2Fe_{14}B$ mainly results from the smaller surface concentration of Nd accompanied by hydrogen-induced Fe enrichment at the surface as discussed later.

In $Nd_2Co_{14}B$, the ratios Nd/Nd_{ox} and Co/Co_{ox} do not change considerably upon hydrogenation, which is in agreement with the data for D_2^+ ion implanted samples presented before. Hydrogen-induced electronic effects are less significant in $Nd_2Co_{14}B$.

3.4. Depth Profiles. Depth profiles have been measured by Ar ion sputtering of $Nd_2(Fe/Co)_{14}B$ alloys in order to study the element distribution in the alloys and potential hydrogen-induced characteristics in the surface near region. Figure 5 shows the concentration ratio c(Fe/Co)/c(Nd) as a function of sputtering depth (which has been roughly estimated from the sputtering parameters) for nonhydrogenated systems (Figure 5a) and for alloys hydrogenated at the temperature of maximum hydrogen absorption (423/573 K, Figure 5b) and quenched from early stages of the disproportionation process (1073 K, Figure 5c), respectively. The profiles demonstrate considerable deviations in the near-surface region from the stoichiometric ratio c(Fe/Co):c(Nd) = 7:1. Preferential sputtering effects play a minor role as can be seen from the fact that the profiles approach this stoichiometric relation in the bulk. The surface near region shows an overall Nd enrichment, which becomes less pronounced and less expanded with increasing Co content of the alloys. Langell et al.[25] already found a similar Nd enrichment in XPS depth profiles of nonhy-

(24) Lebiedz, D.; Züchner, H.; Gutfleisch, O. *J. Alloys Compd.* **2003**, *356−357*, 679.

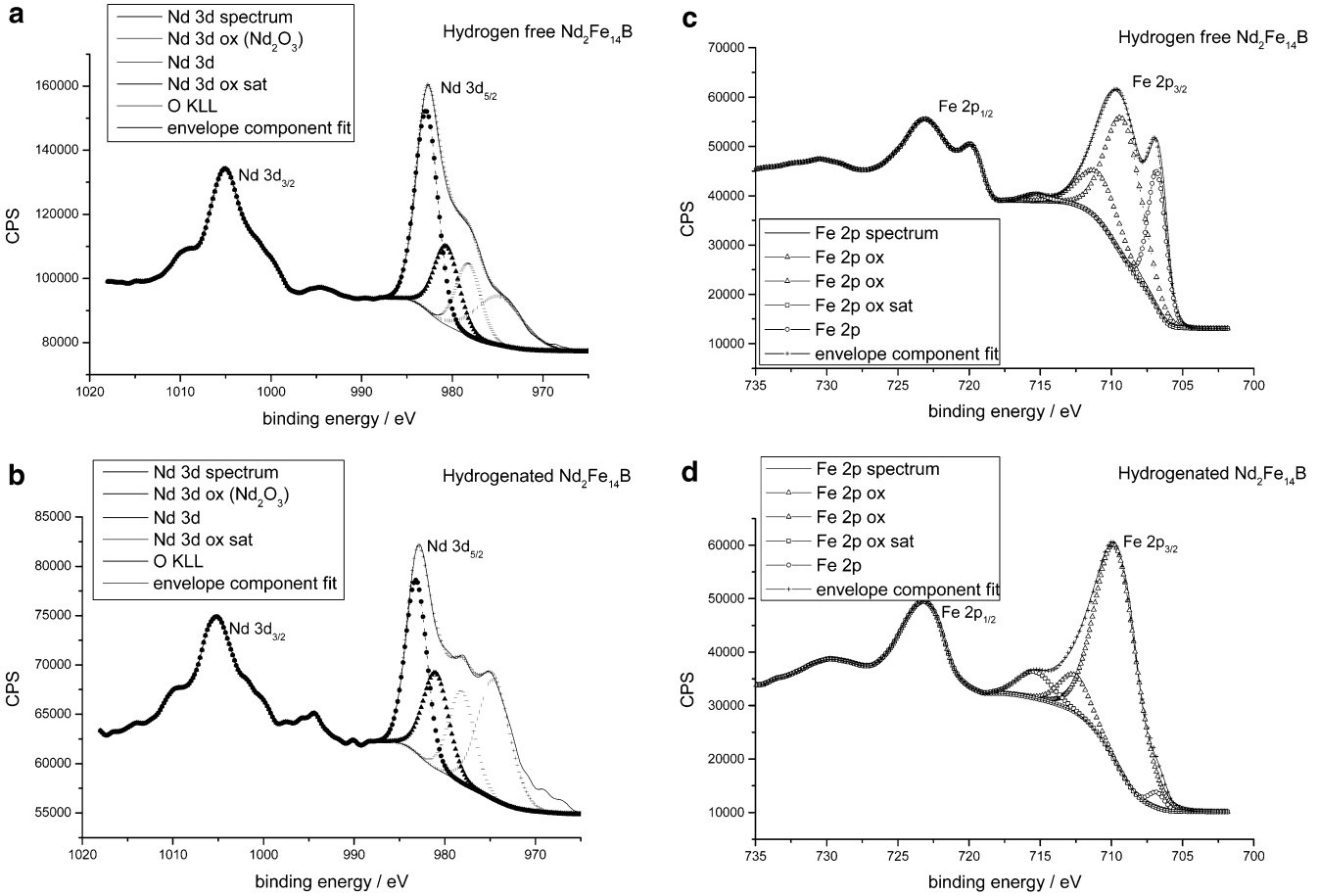

Figure 4. Surface oxidation behavior of hydrogen-free (a) and hydrogenated (423 K, 800 mbar H_2) $Nd_2Fe_{14}B$ (b). The occurrence of the satelite peak (Nd 3d ox sat) is a "final-state effect". This peak corresponds to a $3d^94f^4L^{N-1}$, whereas the main Nd 3d ox peak corresponds to $3d^94f^3L^N$ final state (L denotes the number of valence band electrons).[26−28] Fe 2p region in $Nd_2Fe_{14}B$ (c) and in $Nd_2Fe_{14}BH_x$ (d). Component quantification, see Table 1.

drogenated $Nd_2Fe_{14}B$ and suggested that it is oxygen induced. This hypothesis is supported by the data of the present work taking the oxygen depth profile (not shown) into account, which demonstrates that the Nd enrichment region contains relatively large amounts of oxygen. However, in the outermost surface layers of alloys with significant Fe content, a local relative enrichment of Fe can be observed (see arrows in Figure 5).

These observations give direct information about the reduced hydrogen uptake ability and the increased hydrogenation temperature of Co-containing alloys. As Gutfleisch et al.[11] suggested, a Nd-rich intergranular phase serves as a fast diffusion path for hydrogen. The segregation of Nd to the surface near region therefore favors a fast transport of surface-adsorbed atomic hydrogen into the bulk. The decrease of this Nd enrichment region in alloys with major Co content may be a reason for the reduction of hydrogen uptake capacity in comparison to the Fe alloys. It affects both the diffusion kinetics and the thermodynamic properties of hydrogen alloy interaction. In this context, the preferred binding of hydrogen to Nd is obviously a crucial aspect. The relative Fe enrichment at the outermost surface of iron-rich alloys explains why these alloys have smaller hydrogenation temperatures compared to the cobalt-rich alloys. The absence of a corresponding Co enrichment diminishes the catalytic activity for hydrogen dissociation and inhibits, therefore, the hydrogen uptake by cobalt-rich alloys. Fe is known to be a good catalyst (better than Co) for an effective hydrogen dissociation, which must precede the hydrogen uptake by the alloy. The higher effectivity of Fe as a catalyst for hydrogen dissociation in comparison to Co in the NdFe/CoB system is confirmed in a secondary ion mass spectrometry study of these systems.[24] Figure 5b, which shows the depth profiles of the hydrogenated systems, gives clear evidence for the Nd enrichment in a broad surface near region and additionally a strong Fe enrichment c(Fe):c(Nd) = 10 in the outermost surface layers. The additional hydrogen-induced iron segregation to the outermost surface is the reason for the high and fast hydrogen uptake ability of the Fe-rich alloys.

Table 3 shows qualitatively the same results for the D_2^+ ion implanted systems. The surface concentration ratio c(Fe/c(Nd) increases by a factor 2.5 after hydrogen implantation (Table 3), which supports the argument of a hydrogen-induced Nd 4f intensity increase as an electronic rather than a compositional effect (see section 3.2).

(25) Langell, M. A.; Ren, Y.; Sellmyer, D. J. *J. Magn. Magn. Mater.* **1989**, *82*, 213.
(26) Tanaka, K.; Yamada, M.; Narita, Y.; Takaki, H. *Mater. Sci. Eng.* **1994**, *A181/182*, 932.
(27) Siegmann, H. C.; Schlapbach, L.; Brundle, C. R. *Phys. Rev. Lett.* **1978**, *40*, 972.
(28) Schlapbach, L. *Solid State Commun.* **1981**, *38*, 117.

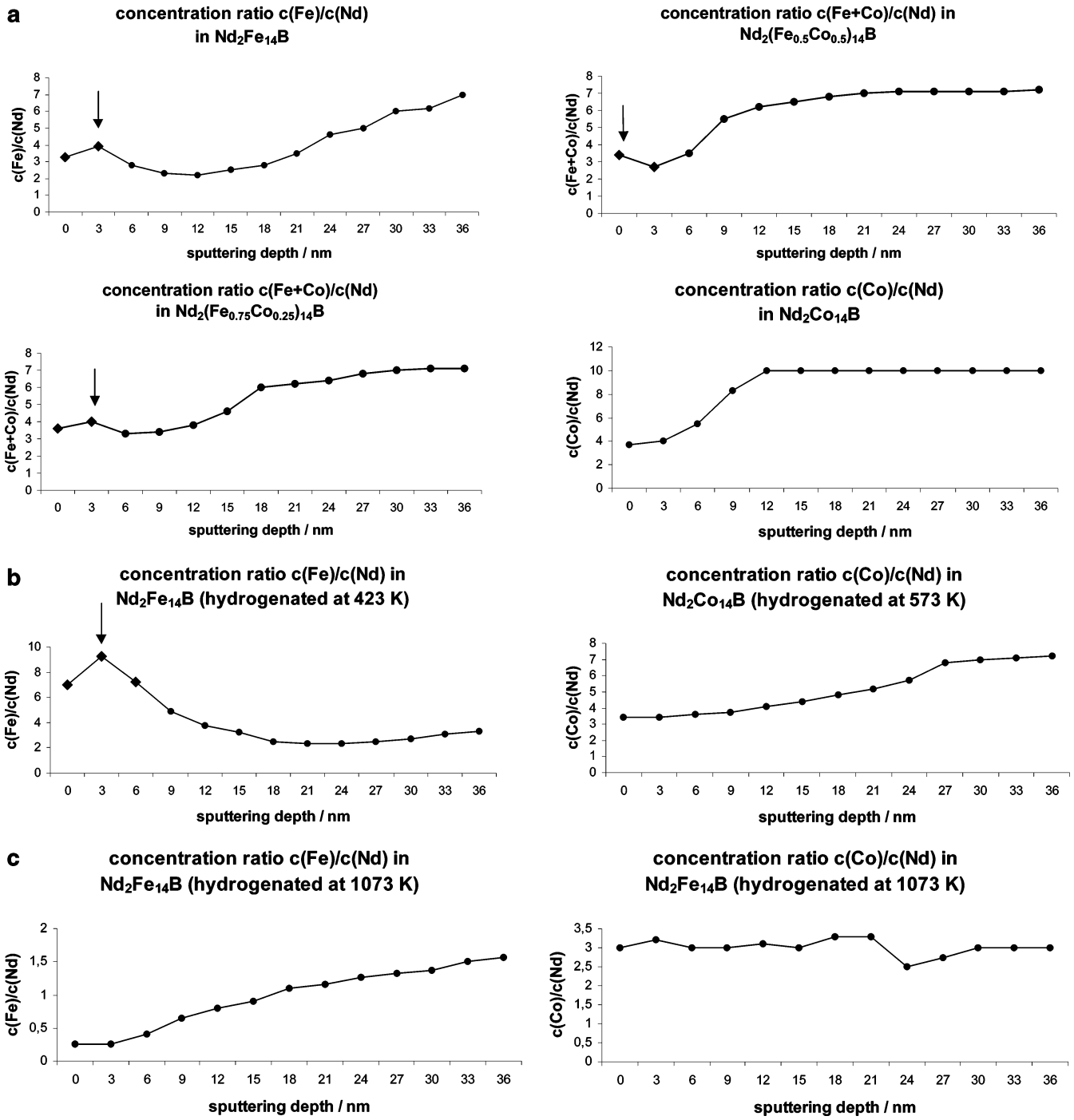

Figure 5. (a) XPS depth profiles of hydrogen free $Nd_2(Fe_xCo_{1-x})_{14}B$; 1) $x = 1$, 2) $x = 0.75$, 3) $x = 0.5$. (b) XPS depth profiles of $Nd_2Fe_{14}B/Nd_2Co_{14}B$ hydrogenated in 800 mbar hydrogen, atmosphere at 423/573 K, (c) XPS depth profiles of $Nd_2Fe_{14}B/Nd_2Co_{14}B$ hydrogenated and partially disproportionated in 700 bar hydrogen atmosphere at 1073 K.

Table 3. Elemental XPS Quantification (%) of Alloys after D_2^+ Ion Implantation

	$Nd_2Fe_{14}B$		$Nd_2Co_{14}B$	
element	nonhydrogenated	hydrogenated	nonhydrogenated	hydrogenated
Fe 2p/Co 2p	76	83	84	80
O 1s	5	8	2	4
C 1s	3	3	1	2
B 1s	7	2	6	6
Nd 4d	9	4	7	8
Fe 3p+Co 3p				

The surface composition of partially disproportionated $Nd_2Fe_{14}B$ und $Nd_2Co_{14}B$ treated in the same way (see section 2; for the disproportionation of $Nd_2Co_{14}B$ reactive milling conditions or high hydrogen pressures are required) is shown in Figure 5c. Almost no surface Fe can be detected in $Nd_2Fe_{14}B$ after partial disproportionation according to the s-HDDR process, which suggests that the separation of the alloy components into surface near Nd and Fe in the bulk is an important step during the disproportionation reaction. This tendency to separation is already observed at lower temperatures of hydrogenation except for the Fe enrichment in the outermost surface layer. Probably the surface catalytic activity of Fe is not required for hydrogen dissociation at the high temperatures (1023 K) of disproportionation. Under these conditions, the degree of oxidation of the

samples due to residual oxygen in the hydrogenation atmosphere is too high to allow the discussion of hydrogen-induced electronic effects at the partially disproportionated stage.

4. Conclusion

The results of the XPS analysis of hydrogen effects in alloys of type $Nd_2(Fe/Co)_{14}B$ permit a better understanding of the behavior of $Nd_2(Fe_xCo_{1-x})_{14}B$ during the HDDR process. The XPS data allow us to interpret the significantly different features of the Fe and Co systems. They provide further information on the characteristics of the hydrogen-induced disproportionation tendency of the Fe-rich alloys and allow further insight into the mechanism of the initial stage of the disproportionation reaction and the stabilizing effect of Co. With respect to both electronic structure and surface composition, hydrogen-induced electronic and segregation effects seem to destabilize the $Nd_2Fe_{14}B$ alloy, which is less stable than $Nd_2Co_{14}B$ even without hydrogen. On one hand, these effects make the Fe alloy suitable for hydrogenation, and on the other hand, they initiate the disproportionation. At the metal surface, this tendency becomes obvious even at low temperatures, albeit under the influence of possible thermal effects due to Ar/D_2^+ surface sputtering. This means, the reactions observed at the surface could reflect the processes taking place in the bulk during the HDDR process.

The Nd−Fe bonding strength in $Nd_2Fe_{14}B$ is weaker than Nd−Co in $Nd_2Co_{14}B$, which inter alia results from the smaller polarity of the chemical bonding. This polarity becomes even weaker under the influence of hydrogen. Deuterium ion implantation under UHV conditions allows the detection of small but in comparison to reference measurements clearly observable electronic effects in the valence band region. Together with the depth profiles, these effects underline the significance of Nd for hydrogen binding and diffusion as well as the role of Fe as an effective surface catalyst for hydrogen dissociation.

The separation of the alloy components into Nd near the surface and Fe closer to the bulk seems to be an important step during the disproportionation process. Almost no surface Fe can be found in the analysis of partially disproportionated $Nd_2Fe_{14}B$. At these high temperatures (1023 K), the surface catalytic activity of Fe is obviously no longer significant for hydrogen dissociation and uptake.

CM021369L